ISSN 1819-7140, Russian Journal of Pacific Geology, 2021, Vol. 15, No. 4, pp. 325–344. © Pleiades Publishing, Ltd., 2021.
Russian Text © The Author(s), 2021, published in Tikhookeanskaya Geologiya, 2021, Vol. 40, No. 4, pp. 51–71.

Granitoids of the Altakhta Complex, the Eastern Part of the Bureya Continental Massif, Central Asian Fold Belt: Age, Geochemical Features, and Geodynamic Interpretations

V. A. Guryanov[a], *, E. V. Nigai[a], Yu. Yu. Yurchenko[c], M. V. Arkhipov[a], S. A. Amelin[b], and V. N. Arapov[b]

[a] *Kosygin Institute of Tectonics and Geodynamics, Far Eastern Branch, Russian Academy of Sciences, Khabarovsk, 680000 Russia*

[b] *JSC Dal'nevostochnoe PGO, Rosgeologiya, Khabarovsk, Russia*

[c] *Karpinskii All-Russia Research Institute of Geology, St. Petersburg, 199106 Russia*

**e-mail: guryanov_v@mail.ru*

Received October 15, 2019; revised December 2, 2020; accepted March 19, 2021

Abstract—New data are reported on the age, composition, and formation conditions of the Late Triassic granitoids of minor intrusions from the eastern part of the Bureya continental massif of the Central Asian fold belt, and their geodynamic interpretation is given. U–Pb geochronological zircon studies indicate that the rocks of the Altakhta syenite–leucogranite complex were formed in two phases within 235–224 Ma. The first phase (235.3 ± 2.9–230 Ma) was responsible for the formation of magmatic rocks that are similar to the A_1-type intraplate granitoids in terms of geochemistry and resemble subduction- and collision- related granitoids in terms of REE composition. The second phase (226–224 Ma) produced granites similar to A_2-type and A_2 + I and S-types. A combination of within-plate and subduction signatures and the presence of A, I, and S-type rocks of similar ages in this complex supports their formation in a transform continental margin setting.

Keywords: Altakhta Complex, granitoids, U–Pb age, zircon, collision, subduction, transform continental margin, Bureya massif

DOI: 10.1134/S1819714021040059

INTRODUCTION

The early Mesozoic intense granitoid magmatism in the eastern part of the Bureya continental massif of the Central Asian Fold Belt (CAFB), along the continent–ocean margin, [16] resulted in the formation of large granitoid massifs [4, 13, 17]. The superposition of magmatic areas of different ages produced the structurally intricate polychronous Eastern Bureya granitic belt [8]. The granitoids of this region have been studied for many years [2, 11, 14, 18, 19, 21, 24]; however, many problems related to the conditions and sequence of their formation remain insufficiently understood. Recent geochronological dating made it possible to ascribe the granitoids of the eastern Bureya belt to the Late Triassic and Late Triassic–Early Jurassic [1, 10]. These granitoids were initially ascribed to Permian, Permian–Triassic, or Jurassic [13, 15, and others]; A.F. Vas'kin later united them in a single Late Permian–Early Triassic Kharin Complex [4], while N.N. Petruk, in contrast, divided them [17] into two independent Middle–Late Triassic Altakhta and Late Jurassic Kharin Complex. A.F. Vas'kin and V.E. Chepygin proposed that the alkaline intrusive rocks of the Altakhta and Kharin complexes are similar in many parameters. On this basis, the Altakhta Complex was excluded from magmatic schemes in the legend of the Bureya Group in the Gosgeolkarta-200 sheets [4]. The criteria for distinguishing these complexes in the absence of reliable geochronological dates seemed to be weakly convincing [15].

Recent geochronological and geochemical studies demonstrated that traditional magmatic schemes for this region, as well as reconstruction of the settings of magmatic activity, require significant revision. The solution of these problems requires the geochronological subdivision of the magmatic activity coupled with geochemical study and, finally, deciphering the geodynamic setting of its formation. The difficulties in studying the magmatism of the Bureya continental massif (BM) of the CAFB can be exemplified by the Turan and Lesser Xingan blocks, which are fragments of a Paleozoic marginal-continental magmatic arc. Their U–Pb geochronological dating revealed the manifestation of Late Triassic Altakhta and Late Triassic–Early Jurassic Kharin granitoid magmatism [1, 10].

Based on new geological, geochronologilcal, and geochemical data, we considered the geological posi-

tion, compositional characteristics, age, and geochemical features of the Late Triassic granitoids of minor intrusions in the eastern BM of the CAFB and gave a geodynamic interpretation. The main study objects were a series of small granitoid massifs in the middle reaches of the Bureya River basin on the left tributary of the Amur River (Fig. 1), which were ascribed by previous researchers to different stages of granite formation [4, 13, 15, 17]. The work is based on materials of field studies, new geochemical data, and results of U–Pb dating of the granitoids of minor intrusions (massifs) in the middle reaches of the Bureya River in the eastern BM coupled with generalization of original data on the Early Mesozoic granitoids of the Altakhta complex.

THE GEOLOGICAL ENVIRONMENT

No less than 70% of the eastern BM is occupied by Paleozoic and Early Mesozoic granitoids. It is generally accepted that the "basement" of this part of the BM is made up of the metamorphic sequences of the Tastakh, Amur groups and Gudzhal and Nyatygran formations, which have been previously considered as Neoarchean and Paleoproterozoic in age [4, 13, 15]. However, new data show that the protoliths of these metamorphic sequences were formed in the Neoproterozoic and (or) Early Paleozoic, while superimposed structural–metamorphic deformations are related to the Paleozoic and Early Mesozoic stages in the geological evolution of the eastern BM [12, 23]. A significant part of the territory is occupied by the granitoid massifs of the Tyrma–Bureya and Kharin complexes, which are ascribed to the Late Paleozoic and Early Mesozoic stages of its geological evolution [4, 17]. The granitoids of the Altakhta Complex are absent in the legend of the Bureya Group in the Gosgeolkarta-200 sheets of the second generation and on most of recently published maps [4, 13]. One characteristic feature of rocks of this complex is the presence of alkaline and subalkaline granites, leucogranites, syenites, granosyenites, pegmatites, quartz syenites, and syenite porphyries, which are associated with the rare-earth–beryllium and uranium–thorium mineralization. The known K–Ar age determinations for these rocks span a range from Late Carboniferous to the Jurassic including [15].

During geological surveying in the middle reaches of the Bureya River basin in 1957–1958, Vasil'eva and Vasil'ev distinguished small intrusive monzonite–syenite–alkaline granite massifs cutting across the Tyrma–Bureya complex [3]. In their composition, L.G. Vasil'eva described alkaline syenites, granosyenites, syenite porphyries, alkaline granites, and vein bodies of grorudites with inclusions of elongated grains of amphibole–riebeckite and aegirine, These bodies are spatially associated with bostonite and selvsbergite dikes. Based on one of the first K–Ar dates obtained at the Laboratory of the Far East Geological Institute, Vladivostok, the age of the alkaline syenites is 230 Ma [3]. Mineralogical–petrographic study of subalkaline and alkaline rocks that compose dikes of grorudites, syenite porphyry, granosyenite porphyry, and pegmatites in the Bureya–Nizhnii Melgin interfluve was carried out for the first time by Rasskazov [20]. Later, these rocks were united into the Altakhta intrusive complex represented by three NE-trending chains of small (from 5 to 50 km^2) stock-like massifs: Altakhta, Ust-Tyrma, Chalbach, Allin, Sularin, and other massifs (Fig. 1), whose total area of which is no more than 150 km^2 [19]. Numerous rock varieties in these intrusions show intricate relationships. Later, more detailed study of these massifs was carried out during large-scale mapping for uranium by Sevast'yanov and Zmievskii [17]. Field studies of the Chalbach and Ust-Tyrma massifs (Fig. 1) allowed Putintsev [19] to divide the Altakhta complex into two intrusive phases of the Late Paleozoic age. Slightly later, similar alkaline rocks were found in the Oktyabr'sk'ii block of the BM, as well as in the exposed basement in the Amur–Zeya basin. Yu.P. Zmievskii determined their age as Triassic. The older Late Triassic age of the granitoids of minor intrusions compared to rocks of the Kharin Complex was determined by U–Pb zircon dating during preparation of sheet M-52-XII of Gosgeolkarta-200/2 (Fig. 2) [1].

The massif in the Bol. Aimka River mouth, which was studied in different years by V.G. Gonevchuk and A.M. Kokorin [6–8], is of special interest. It is composed of medium to coarse-grained microcline granites exposed in the Bol. Aimka–Malaya Aimka interfluve, near their emptying into the Niman River (Fig. 1). They differ from typical Kharin granites in their higher agpaitic index, predominance of alkaline rocks, K predominance over Na, and extremely low contents of Mg and Ca. They were classified as the A-type anorogenic within-plate granites with admixture of sedimentogenic (S-type) granites [6–8]. It is important that their K–Ar biotite, muscovite, and hornblende ages of 225–235 Ma [8] coincide with obtained Late Triassic age of the Altakhta Complex [1, 10]. Therefore, we ascribe them to the rocks of the Altakhta Complex.

THE GEOLOGICAL POSITION AND COMPOSITION OF THE GRANITOIDS

The Altakhta granitoid massifs are the widest spread in the basins of the Sularin, Nizhnii, and Verkhnii Melgin rivers, in the upper reaches of the Talaya and Tuyun rivers, and in the lower reaches of the Bol. Aimka and Mal. Aimka rivers, occupying a significant part of the middle reaches of the Bureya River (Figs. 1, 2). They cut across Neoproterozoic metamorphic sequences and Early Paleozoic biotite and two-mica granites of the Kivili and Sularin complexes, and the Devonian–Permian volcanic rocks of the Amgan and Permian–Triassic granitoids of the

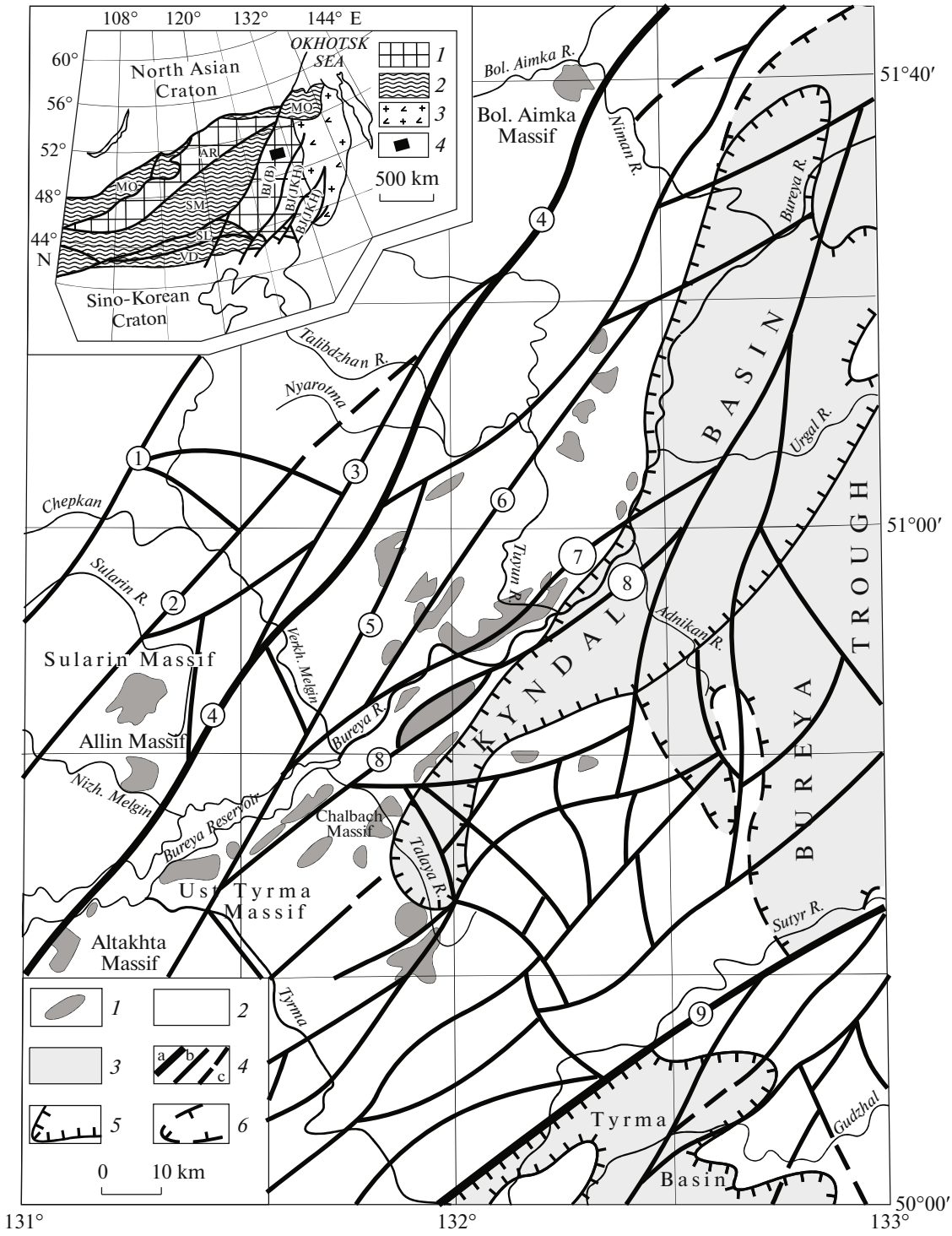

Fig. 1. The scheme of the location of the Late Triassic granitoid intrusions of the Altakhta Complex (compiled using materials by Yu.P. Rasskazov, 1959; V.V. Vasil'eva, 1960; A.S. Sevast'yanov, 1968; V.K. Putintsev et al., 1970; V.G. Yu.P. Zmievskii, 1982; M.V. Martynyuk et al., 1983; and Gonevchuk et al., 1995) . (*1*) Granitoid massifs of the Altakhta Complex and their names; (*2*) undivided Phanerozoic and Precambrian magmatic and metamorphic complexes in the eastern BM; (*3*) complexes of sedimentary and volcanosedimentary rocks of the Kyndal Basin and Bureya Trough; (*4*) faults: (a) major (regional), (b) subsidiary, (c) inferred. (*5–6*) Contours of the basin (*5*) and trough (*6*). Faults: (1) Chepkan, (2) Sularin, (3) Chergilen, (4) Melgin; (5) Nyatygran–Telemdzha, (6) Yanyr, (7) Pribureya, (8) Bureya, (9) Xingan. Inset shows the position of the studied area in the eastern part of the Central-Asian Fold Belt (tectonic basis after [13], modifications after [23]): (*1*) superterranes: (AR) Argun, (BJ) Bureya–Jiamusi (BJ), (B) Bureya terrane (continental massif), BJ (JKH) Jiamusi–Khanka terrane (continental massif); (*2*) Paleozoic–Early Mesozoic fold ((SM) South Mongolian, (SL) Solonker, (VD) Vundarmiao, (MO) Mongol–Okhotsk), (*3*) Late Jurassic–Early Cretaceous orogenic belts; (*4*) studied area.

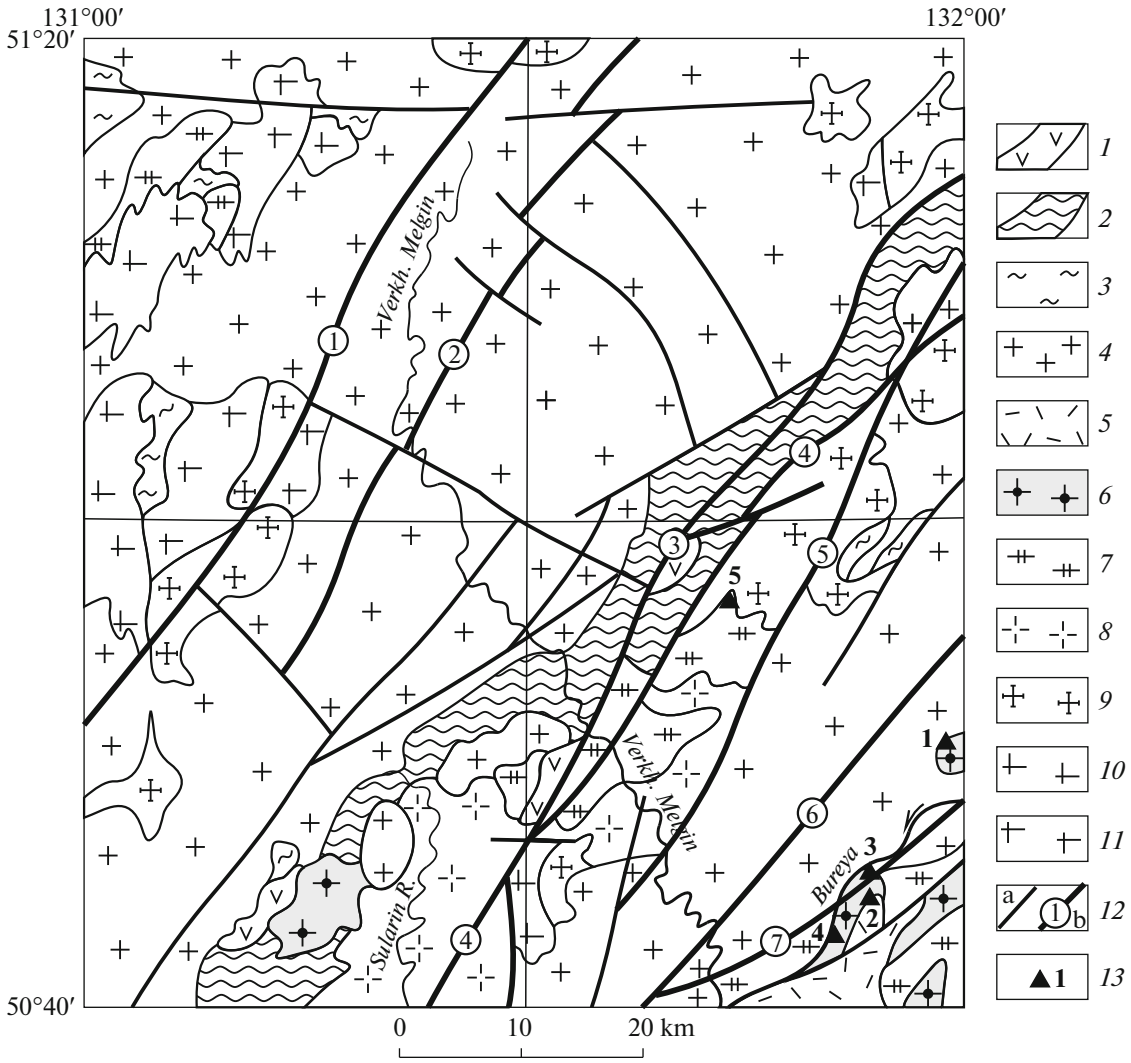

Fig. 2. Geological scheme of the Verkhnii Melgin River basin (simplified after [1]). (*1*) Devonian–Permian (?) volcanic rocks of the Amgan Complex; (*2*) Late Neoproterozoic–Paleozoic volcanogenic–carbonate–terrigenous rocks of the Melgin Trough; (*3*) Precambrian gneisses and crystalline schists (salient of crystalline basement); (*4*) Late Triassic–Early Jurassic granitoids of the Kharin Complex; (*5*) Late Triassic trachyrhyolites of the Talovsky Complex; (*6*) Late Triassic syenites, quartz syenites, alkaline granites, and granosyenites, subalkaline granites and leucogranites of the Altakhta Complex; (*7*) Late Permian–Early Triassic granitoids of the Tyrma–Bureya Complex; (*8*) Early Ordovician granites of the Sularin Complex; (*9*) Cambrian–Early Ordovician granitoids of the Kivili Complex: (*10*) Neopaleoproterozoic granitoids and gabbroids of the Nyatygran Complex; (*11*) Precambrian ultrametamorphic granites of the Drevnyaya Bureya Complex; (*12*) faults: (a) subordinate and (b) major ((1) Chepkan, (2) Yugormin, (3) Chergilen, (4) Melgin, (5) Nyatygran-Telemdzhan, (6) Yanyr, (7) Pribureya); (*13*) geochronological sampling localities and their numbers in Tables 3–6.

Tyrma–Bureya complex [1]. The massifs of the Altakhta granitoids have an irregular E–W, more rarely NE-extended shape; in the areas of their largest development they are grouped into the NE-trending chains controlled by tectonically weakened zones [1]. The body sizes vary from 1–3 to 65 km^2. Some massifs have a simple structure and consist of quartz syenites, which in the inner contact zones grade into syenite porphyries. The syenite porphyry fringe reaches 200–400 m thick at a gentle dip of contacts and is absent at steep (>50°) contacts.

Some massifs have a clearly expressed two-phase structure. In particular, the hornblende syenites of the Chalbach massif are intruded by leucogranites and subalkaline granites of the second phase [17]. Aegirine and aegirine–riebeckite syenites and granites developed at the contact with host metadolerites with increasing distance are replaced by syenites. Other intrusions are widely developed to the east, south, and southeast of the Melgin Trough and are close in size to the above-mentioned massifs. They usually have an elongate shape and are grouped into NE-trending chains (Figs. 1, 2). Massifs in the Bureya–Tyrmak

interfluve have a different structure. They are made up of inequigranular pyroxene–hornblende syenites and quartz monzonites with marginal facies represented by fine-grained alaskitic and subalkaline amphibole granites. A massif in the upper reaches of the Talaya River shows zoning expressed in a change from quartz syenites to granosyenites on one flank and to fine-grained moderately alkaline granites within a 1–5 km wide band on the other flank. In this area, in the Talaya River basin, the rocks of the Altakhta complex are intruded by subvolcanic trachyrhyolites of the Talovsky and Early Jurassic leucogranites of the Kharin complexes [1].

Magnetic and gravity survey and deep seismic sounding of this territory of the BM showed that the Moho topography is complicated by an extended NE-trending trough, which was interpreted as the trace of a regional transcrustal fault rooting deeply in mantle [1]. On the surface, this fault is likely marked by the outcrops of the Altakhta granitoids. Their NE-orientation and linear morphology of exposures indicate a direct relation of intrusive activity with faults (Figs. 1, 2). It should be noted that the chains of small massifs are extended in the NE direction along the Sularin, Chergilen, Melgin, Nyatygran–Telemdzha, Yanyr, Pribureya, and Bureya faults (Fig. 1). At the surface and in the upper crust, the mantle-rooted fault is marked by the above-mentioned faults and NE-trending intrusion chains tracing them.

Generalization of available and new data showed than many intrusions were formed in two phases [1]. The first phase includes syenites, quartz monzonites, quartz syenites, granosyenites, alkaline granites, and leucogranites, alkaline syenites, and quartz syenites. The second phase comprises subalkaline leucogranites and granites, leucogranite porphyries, dikes of granite porphyries and subalkaline leucogranites, as well as veins of aplites, aplite-like granites, and pegmatites.

The main objects of our study were granites, leucogranite porphyries, granosyenites, quartz syenites, and syenite porphyries of small intrusions in the Pivovarovskii Creek basin and Sularin–Shirokaya interfluve on the right and left banks of the middle reaches of the Bureya River (Fig. 2). These are mainly fissure bodies of subalkaline leucogranites and quartz syenites from 3.5 to 8 km long at a width up to 2 km, which trace NE-trending deep-seated fault zones (Fig. 1). It was established that they are overlapped by Late Triassic volcanic rocks of the Talovsky Complex (218.1 ± 2.8 Ma, U–Pb, zircon) and are intruded by the Kharin granites (199.0 ± 4.0 Ma) [1, 46]. In this area, they cut across granitoids of the Tyrma–Bureya, Kivili, and Nyatygran complexes. The body contacts are either inclined to the southeast or are steep and linear. The intrusions have a heterogeneous composition. Some of them consist of granosyenite central part and quartz syenite or subalkaline granite and leucogranite margins. Other bodies are composed of granites or granosyenites alone. In particular, the Vodorazdel'nyi intrusion 41 km^2 in area in the Sularin–Shirokaya interfluve is composed mainly of the granosyenites of the first phase. The largest massif in the Sularin–Nizhnii Melgin interfluve 63.8 km^2 in area is composed mainly of syenites, granosyenites, quartz monzonites, and quartz syenites of the first phase. The petrotypical Sularin massif 25 km^2 in area is located southwest, in the middle reaches of the Nizhnii Melgin River and consists of two phases. The subalkaline granites and leucogranites of the second phase intrude the granosyenites, quartz monzonites, and syenites of the first phase. The massifs are associated with aplite and pegmatite veins and dikes of granite porphyries with characteristic pitch black quartz (upper reaches of the Adnikan River), syenite porphyries, granosyenite porphyries, more rarely grorudites, bostonites, and selvsbergites. The dikes are from 1–2 to 10 m thick and up to 300 m long. The rocks of the complex are characterized by a lilac-pink, reddish-pink, reddish-gray color; quartz syenites only sometimes acquire a pinkish yellow color.

The massifs of the Altakhta granitoids located among the Neoproterozoic and Cambrian rocks are surrounded by aureoles of ocellar and spotty cordierite schists. The host rocks are usually Paleozoic granitoids, which were silicified, albitized, and limonitized at the contact with the massifs.

The granitoids of the first phase of the complex comprise a large group of variegated rocks dominated by syenites, granosyenites, alkaline granites, quartz syenites, granosyenites, and alkaline leucogranites. They frequently contain alkaline amphibole and pyroxene.

Syenites are medium-grained subhedral massive rocks with elements of monzonitic texture [1, 3, 19]. The mineral composition is as follows (in wt %): quartz (0–5), microcline–microperthite (rarely, orthoclase) (65–75), albite–oligoclase no. 5–25 (10–25), biotite, bluish-green hornblende, clinopyroxene (5–15), rarely aegirine–augite. Accessory minerals are apatite, titanite, titanomagnetite; secondary minerals are albite, epidote, and limonite.

The alkaline quartz syenites, alkaline granosyenites (small massifs in the near-mouth part of the Tuyun River and in the upper reaches of the Adnikan River after [3, 17, 19, 20]) are coarse- or medium-grained massive rocks with pegmatoid groundmass. They have the following mineral composition (in wt %): albite or albitized oligoclase (20–40), albitized microcline-perthite (40–50), bluish green hornblende (1–10), arfvedsonite (3–5), riebeckite (3–5), aegirine augite (1–10); dark smoky to black quartz (5–15), and miarolitic cavities. Accessory minerals are monazite, xenotime, apatite, fergusonite, and small clusters of titanomagnetite; secondary minerals are K-feldspar, albite, epidote, and chlorite.

The alkaline granites (after [3, 17, 20]) are medium to coarse-grained taxitic and massive rocks with a pegmatoid, locally poiklitic texture. They are mainly represented by porphyritic varieties with pocket distribution of mafic minerals. The granites are made up (in wt %) of perthitic K-feldspar (55–60), albite (15–20), quartz (10–25), riebeckite (1–10), aegirine (0–5), and more rarely arfvedsonite. Accessory minerals are zircon, apatite, titanomagnetite, and monazite; secondary minerals are albite and chlorite.

The alkaline leucogranites (polished thin section 1173-1, Berezovyi creek [1]; massif of the Bol'shaya Akimka River basin: samples GN-1, 2, 6 [8]) consist of coarse-grained massive rocks with pegmatoid groundmass. The mineral composition of the alkaline leucogranites is as follows (in wt %): albitized microcline-perthite (50–55), albite or albitized oligoclase (15–20), quartz (30), rare aegirine–arfvedsonite (ekerite), polylithionite, and riebeckite. Accessory minerals are zircon, monazite, apatite; secondary minerals are albite, hematite, and limonite.

The granosyenites, quartz syenites (polished thin sections 316201, after [1, 20]) are medium- to fine-grained, sometimes porphyritic rocks with hypidiomorphic texture. They consist of the following minerals (in wt %): quartz (10–20), microcline-perthite (rarely orthoclase) (50–70), albite–oligoclase (10–30), biotite (up to 5), bluish green hornblende (up to 5), sometimes, aegirine arfvedsonite. The granosyenites show elements of graphical structure and quartz xenomorphism. Accessory minerals are zircon, apatite, titanite, allanite, epidote, and magnetite. Secondary chlorite is developed after biotite.

The second phase is represented by subalkaline leucogranites, granites, and leucogranite porphyries, as well as by granite porphyry and leucogranite dikes, and veins of aplites, aplitic granites, and pegmatites.

The subalkaline leucogranites are medium to fine-grained massive porphyritic rocks (polished thin sections 11500, 10202, after [1, 17]) consisting (in wt %) of prismatic oligoclase (15–20), microcline (55–60), equant quartz (25–30), single bluish green hornblende and biotite flakes. The groundmass is hypidiomorphic, locally micropegmatitic, with elements of poikilitic texture. Accessory minerals are monazite, allanite, zircon, and magnetite. The hornblende is replaced by chlorite, while feldspars are replaced by albite, sericite, and pelite.

The subalkaline porphyritic granites (polished thin sections 107701, 117300) and granite porphyries (after [1, 3, 17]) have micrograined poikilitic groundmass. Phenocrysts (40%) are represented by pure quartz (15%) in a limonite coat, tables (up to 6 mm) of pelitized K-feldspar (10–25%) and K-feldspathized plagioclase (0–15%), scarce magnetite (2 mm) forms pseudomorphs after mafic minerals (relict fragments of biotite and hornblende). The groundmass (60%) is made up of quartz, pelitized K-feldspar, plagioclase, zircon, apatite, and irregular clusters of ore minerals. Secondary minerals are limonite, sericite, K-feldspar, muscovite, and epidote.

Pegmatites (after [3, 19, 20]) are made up of blocky aggregates of microcline and quartz (up to 5 cm across) cemented by quartz mass with biotite, tourmaline, pockets of zircon and monazite, and prismatic allanite up to 3-mm long. Pegmatites contain morion crystals up to 7-cm long.

METHODS

Complete chemical analysis was made for five granitoid samples (Table 1) taken for isotope-geochronological studies. We also used results of silicate analyses of 14 granitoid samples from published (7 samples) and unpublished (TFGI Dal'geologiya, 7 samples) works (Tables 1, 2). The contents of major elements were determined at the Central Laboratory of JSC Dal'geofizika according to OST 41-08-249-85. The contents of trace and rare-earth elements were determined by ICP-MS at the Khabarovsk Innovation–Analytical Center of the Kosygin Institute of Tectonics and Geophysics of the Far Eastern Branch, Russian Academy of Sciences (Khabarovsk) on an Elan 9000 ICP-MS mass-spectrometer (Canada) (analysts A.V. Shtareva and Yu.A. Lushnikova). A relative error in the ICP-MS determination of trace and rare-earth elements was no more than 5%.

The separation and study of zircons were carried out at the Center of Isotopic Research (CIR) of VSEGEI (St. Petersburg). Samples were crushed, separated into fractions, then the fraction less than 0.25 mm was passed through a centrifugal ITOMAK-KN-0.1 concentrator. The obtained heavy fraction was subjected to electromagnetic separation and then was finally purified in a heavy liquid. Several tens of grains were hand-picked from obtained concentrate under binocular microscope and most typical of them were used for isotope studies. U–Pb zircon dating was carried out on an SHRIMP-II ion microprobe at the CIR of VSEGEI. The selected zircon grains together with TEMORA and 91500 zircon standards were mounted in epoxy and then polished to about half their thickness. Optical (in transmitted and reflected light) and cathodoluminescence images reflecting the inner structure and zoning of zircon were used to select areas (points) for dating on the zircon surface. The U–Pb measurements on a SHRIMP-II were carried out using technique described in [45]. The intensity of primary beam of molecular negatively charged oxygen ions was 2.5–4 nA, with crater diameter of 15×10 μm and depth of 3–4 μm.

The data were processed using a SQUID software [36]. U–Pb ratios were normalized to 0.0668 assigned to the TEMORA zircon standard, which corresponds to its age of 416.75 Ma [30]. Errors of single analyses (ratios and ages) are given at 1σ level, and errors of cal-

Table 1. Chemical composition of the representative samples of the granitoids of the Altakhta Complex

Sample no.	**117300**	**107701**	**11500**	**10202**	**316201**	GN-1	GN-2	GN-3	GN-4	GN-6
Component	Granitoids of the second phase				Granitoids (syenitic rocks) of the first phase					
SiO_2	74.14	74.73	77.00	76.70	63.30	76.75	76.30	78.35	69.35	72.00
TiO_2	0.16	0.10	0.06	0.05	1.00	0.69	0.39	0.70	0.66	0.48
Al_2O_3	13.00	12.94	12.34	12.42	14.68	12.20	11.30	11.83	14.85	15.57
Fe_2O_3	1.41	1.35	0.31	1.24	3.02	0.42	0.43	0.19	0.86	0.78
FeO	0.66	0.42	0.81	0.51	4.11	0.62	1.00	0.34	1.98	0.97
MnO	0.02	0.31	0.01	0.09	0.22	0.01	0.02	0.01	0.06	0.09
MgO	0.50	0.50	0.50	0.31	2.37	0.00	0.00	0.06	1.31	0.09
CaO	0.98	0.83	0.50	0.50	2.78	0.46	0.40	0.30	2.49	0.17
Na_2O	3.88	3.89	4.00	3.51	2.94	3.12	2.80	4.02	3.35	5.10
K_2O	4.00	4.58	4.40	4.51	3.47	5.40	6.10	3.54	3.91	4.33
P_2O_5	0.04	0.02	0.10	0.03	0.22	–	–	–	–	–
L.O.I.	0.45	0.34	0.31	0.12	0.68	0.32	0.49	0.16	0.53	0.52
∑	99.24	99.64	100.34	99.99	99.77	100.12	99.33	99.70	99.39	100.19
Li	5.72	6.06	3.23	11.47	–	–	–	–	–	–
Be	2.71	2.67	2.58	2.69	–	–	–	–	–	–
B	1.29	1.01	0.46	0.36	–	–	–	–	–	–
P	115.93	148.34	202.28	290.05	–	–	–	–	–	–
Sc	1.63	1.87	2.32	1.32	–	–	–	–	–	–
Ti	769.31	601.49	437.04	297.03	–	–	–	–	–	–
V	7.91	3.03	3.32	1.34	–	–	–	–	–	–
Cr	8.73	96.11	154.50	101.41	–	5	4	–	–	–
Mn	139.34	166.25	169.64	182.14	–	5	4	0	59	0
Co	1.53	3.05	15.08	11.97	–	2	2	0	11	2
Ni	4.87	22.18	77.32	29.61	–	6	7	5	29	5
Cu	4.91	9.01	11.92	7.96	–	–	–	–	–	–
Zn	36.78	24.36	22.30	23.09	–	–	–	–	–	–
Ga	19.75	19.22	19.25	17.42	–	–	–	–	–	–
Ge	1.36	1.23	1.36	1.01	–	–	–	–	–	–
As	5.87	4.80	4.53	4.47	–	–	–	–	–	–
Rb	160.50	190.05	189.33	207.00	–	475	470	165	190	480
Sr	57.45	50.03	5.15	41.18	–	36	32	14	410	44
Y	21.58	18.03	15.69	8.53	–	61	60	83	27	62
Zr	110.24	128.28	123.45	56.20	–	681	792	766	415	651
Nb	18.43	19.41	21.41	16.14	–	0	23	34	0	20
Mo	1.05	1.98	3.26	1.28	–	–	–	–	–	–
Ag	0.35	1.04	0.85	2.58	–	–	–	–	–	–
Cd	0.04	0.03	0.01	0.02	–	–	–	–	–	–
Sn	2.77	4.01	2.61	5.01	–	–	–	–	–	–
Sb	0.22	0.20	0.10	0.19	–	–	–	–	–	–
Cs	1.15	1.18	1.27	1.58	–	3.5	5.6	5.7	5.5	3.5
Ba	101.59	98.09	9.08	79.37	–	130	120	24	600	80
La	18.20	30.23	12.90	12.90	53.23	31	41	8	32	40
Ce	45.22	66.82	43.80	31.40	139.06	65	82	18	61	94
Pr	5.64	7.33	4.20	3.65	11.91	8	10	3	8	10
Tb	0.68	0.70	0.53	0.49	1.48	1.17	1.32	1.82	0.64	1.33
Sm	4.75	4.70	3.64	2.64	8.15	6	7	5	5	7

Table 1. (Contd.)

Sample no.	**117300**	**107701**	**11500**	**10202**	**316201**	GN-1	GN-2	GN-3	GN-4	GN-6
Component	Granitoids of the second phase				Granitoids (syenitic rocks) of the first phase					
Dy	3.82	3.74	3.60	3.31	8.50	8	9	14	4	9
Nd	20.52	24.87	15.90	13.90	40.79	25	34	11	26	33
Eu	0.16	0.26	0.04	0.07	0.72	0.32	0.31	0.03	1.01	0.25
Gd	4.59	5.06	3.38	2.72	10.06	–	–	–	–	–
Ho	0.78	0.74	0.83	0.74	1.78	1.80	2.13	3.31	0.75	2.18
Er	2.41	2.16	2.67	2.49	5.28	6	7	12	2	8
Tm	0.38	0.32	0.38	0.40	0.83	1.09	1.26	2.24	0.34	1.43
Yb	2.52	2.00	2.90	3.02	5.32	8	9	17	2	11
Lu	0.38	0.30	0.45	0.41	0.84	1.23	1.39	2.68	0.54	1.74
Hf	4.31	4.33	5.31	2.54	–	–	–	–	–	–
Ta	1.34	1.68	1.78	1.65	–	–	–	–	–	–
W	2.79	33.98	59.16	58.21	–	–	–	–	–	–
Hg	1.30	2.02	2.22	2.14	–	–	–	–	–	–
Tl	1.40	1.66	1.73	1.87	–	–	–	–	–	–
Pb	20.10	50.13	50.89	35.13	–	59	51	81	30	39
Bi	0.47	0.21	0.02	0.13	–	–	–	–	–	–
Th	22.85	29.16	17.55	25.44	–	51	69	29	21	89
U	4.68	5.05	5.53	3.62	–	11	17	34	6	10

Contents of major elements are given in wt %, trace elements, in ppm. Author's data: (117300, 107701) porphyritic subalkaline granites; (11500, 10202) porphyritic subalkaline leucogranites; (316201) quartz syenites. Compositions of rocks of the Bol. Aimka River (after [7, 8]): (GN-1, GN-2) coarse-grained alkaline leucogranites; (GN-3) fine-grained biotite leucogranites; (GN-4) porphyritic biotite–amphibole granites; (GN-6) alkaline leucogranites. Sample numbers correspond to the inventory numbers of those in the Funds of the TFGI Dal'geologiya. Bold type shows sample numbers of granitoids dated by U–Pb zircon method. Dash means not analyzed. (L.O.I). loss on ignition, (Σ) total.

Table 2. Chemical composition (wt %) of the granitoids of the first phase of the Altakhta Complex in the middle reaches of the Bureya River basin according to data by different researchers

Oxides	946	5676	5581	1649-3	5537-2	5621-1	P-1	1664	1687-6
SiO_2	61.33	73.76	63.10	73.66	73.30	75.65	68.02	63.49	67.54
TiO_2	0.75	0.12	0.46	0.14	0.14	0.10	0.32	0.26	0.37
Al_2O_3	14.98	13.72	17.20	13.96	13.56	12.48	16.01	20.72	17.82
Fe_2O_3	4.90	1.61	2.41	0.96	0.61	1.43	1.78	1.49	1.03
FeO	4.92	0.37	2.13	1.19	1.28	0.49	2.06	1.50	2.00
MnO	0.21	0.03	0.09	0.04	0.05	0.02	0.15	0.08	0.07
MgO	0.45	0.16	0.37	0.21	0.40	0.24	0.21	0.44	0.28
CaO	1.58	0.24	1.48	0.18	0.59	0.15	0.83	1.34	0.88
Na_2O	5.09	4.72	4.98	4.82	4.60	4.47	5.02	4.14	4.41
K_2O	3.92	4.68	7.25	4.57	4.57	4.87	5.23	6.18	5.43
H_2O	–	0.27	0.43	0.32	0.39	0.26	–	–	–
P_2O_5	0.13	0.0	0.04	0.01	0.01	–	–	–	–
L.O.I.	–	–	0.43	0.32	0.39	0.26	0.00	0.57	0.34
Σ	99.72	99.68	99.94	100.06	99.51	100.16	99.63	100.21	100.17

(946) quartz syenites, (5676) alkaline granites (Amelin, 2014, TFGI Dal'geologiya funds, inv. no. 891011); (5581) alkaline syenites, (1649-3, 5537-2, and 5621-1) alkaline granites (Yu.P. Zmievskii, TFGI Dal'geologiya funds, inv. no. 19606); (P-1) granosyenites [18]; (1664) alkaline syenites [3], (1687-6) alkaline quartz syenites [3]. Dash means not analyzed. Inventory numbers are given according to reports of TFGI Dal'geologiya funds. (L.O.I.) Loss on ignition, (Σ) Total.

culated concordant ages and concordia intercepts are given at 2σ. Concordia plots were constructed using an ISOPLOT/EX software [35].

THE PETROGEOCHEMICAL CHARACTERISTICS OF THE GRANITOIDS

The chemical composition of the Altakhta granitoids is shown in Tables 1, 2 and Fig. 3. In the SiO_2–(K_2O + Na_2O) classification diagram [34], the rocks of the complex are plotted in the fields of alkaline syenites, alkaline quartz syenites, alkaline granites and leucogranites, quartz syenites, granosyenites, moderately alkaline granites, and granites of normal alkalinity after [29]. In terms of petrochemistry, they correspond to the rocks of the moderate and normal alkalinity, more rarely to the K–Na alkaline rocks [34] with elevated K_2O (up to 7.25 wt %) (Table 2).

The rocks of the first phase are represented by alkaline syenites (SiO_2 63.10–63.49 wt % and total alkalis 10.32–12.23 wt %, respectively) and quartz syenites (67.54 and 9.84 wt %), alkaline granites and leucogranites (72.0–76.07 and 8.52–9.43 wt %), granosyenites (68.02 and 10.25 wt %), and quartz syenites (61.33– 63.30 and 6.41–9.01 wt %). They have high alkali contents and extremely low concentrations (frequently close to zero) of MgO and CaO, which is reflected in their moderate- and high-Al, agpaitic, ferroan compositions and elevated Ti content (Tables 1, 2). In the SiO_2–K_2O diagram [40], their data points fall in the fields of high-K and ultra-K compositions, and their high FeO*/MgO ratios from 2 to 20 could indicate their affiliation to the tholeiitic series [44].

The subalkaline granites (moderately alkaline after [29]) (SiO_2 74.14–74.48 wt % and total alkalis 7.8–8.47 wt %) and subalkaline leucogranites (normally alkaline after [29]) (76.7–77.00 and 8.02–8.40 wt %) of the second phase are characterized by the moderate alkali contents, elevated MgO, CaO, and FeO^{tot} contents, and low TiO_2 (Table 1). Their mineral composition is characterized by the presence of biotite, alkaline (bluish-green) hornblende, and magnetite. They are moderate-Al and weakly peraluminous granites. In the SiO_2–K_2O diagram [40] their data points fall in the fields of high-K rocks.

In the $Fe_2O_3^* \times 5$–(Na_2O + K_2O)–(CaO + MgO) × 5 (Fig. 3a) discriminant diagram recommended by Grebennikov to recognize *A*-type granites of different geodynamic settings [9, 28], the compositions of the Altakhta granitoids (SiO_2 > 67 wt %) are divided into two types: A_1 and A_2+ *I* & *S;* one sample falls into the field of *I* & S-type granites (likely, owing to remelting of magmatic and sedimentary rocks). Based on the interpretation of this diagram, the rocks of the first phase located in the field of A_1-type granites were formed under conditions of within-plate setting near divergent boundaries of the eastern BM (lithospheric plate) in cold intracontinental rifts. The granites of the second phase in the same diagram plot in the fields of A_2-type and joint A_2+ *I* & *S*-types, which may indicate a significant crustal contribution in their formation due to the intense interaction of mafic mantle-derived melts with felsic continental material (A_2) [9, 28]. In the Zr–10000×Ga/Al diagram [44], data points of their compositions are confined to the *A*-type granite field (Fig. 3b). It should be noted that the elevated Ga/Al ratios in the granites of the second phase are characteristic feature of *A*-type melts [9].

According to the Frost [33] and Mayeda [37] classifications, the rocks of the first phase with high FeO*/(FeO* + MgO) = 0.88–1.00 (Fig. 3c) are determined as *A*-type granites. One sample falls in the field of magnesian rocks (likely derived through remelting of magmatic or sedimentary rocks). Their Fe mole fraction is the main petrochemical parameter in distinguishing A-type granites [9]. Unlike the granites of the first phase, the composition points of the granites of the second phase fall in the fields of both ferroan and magnesian rocks FeO*/(FeO* + MgO = 0.67–0.83) (Tables 1, 2), plotting along the discriminant line between them (Fig. 3c). In general, their compositional peculiarity corresponds to the mineralogical characteristics of rocks of two phases of the Altakhta complex, which is caused by the presence of calcium amphibole or alkaline amphibole and pyroxene. In the ANK–ACNK diagram [38], data points of granitoids of the first phase fall in the field of metaluminous and peraluminous rocks, while the rocks of the second phase are in the field of metaluminous rocks (Fig. 3d). In the classification diagram by Whalen [44], data points of the first phase are plotted in the *A*-type field, while granites of the second phase are in the field of nonfractionated and fractionated granitoids of the *I*- and *S*-types (Fig. 3e). In the Pearce discriminant diagram [39] (Fig. 3f), data points of the rocks of the first phase fall in a field of syncollisional and within-plate granites, while granites of the second phase are in a field of syncollisional, within-plate, and volcanic-arc granites.

The geochemical peculiarity of the Altakhta granitoids is their general depletion in REE (Table 1, Fig. 4a), whose concentrations vary from 161 to 282 ppm in the rocks of the first phase and from 77 to 146 ppm in the granites of the second phase. These contents are much lower than those of within-plate granites, but are close to those in collisional and subduction granites (after [5]). The REE distribution pattern in them (Fig. 4c) is almost identical to that of the average crust [25]. The calculated average Sm/Nd ratio (0.21) in the rocks of the Altakhta Complex is lower than in the lower crust (0.27), but higher than in the upper crust (0.173).

The rocks of the Altakhta Complex have high REE contents, LREE enrichment, flat HREE, and deep Eu anomaly in the chondrite-normalized pattern, which

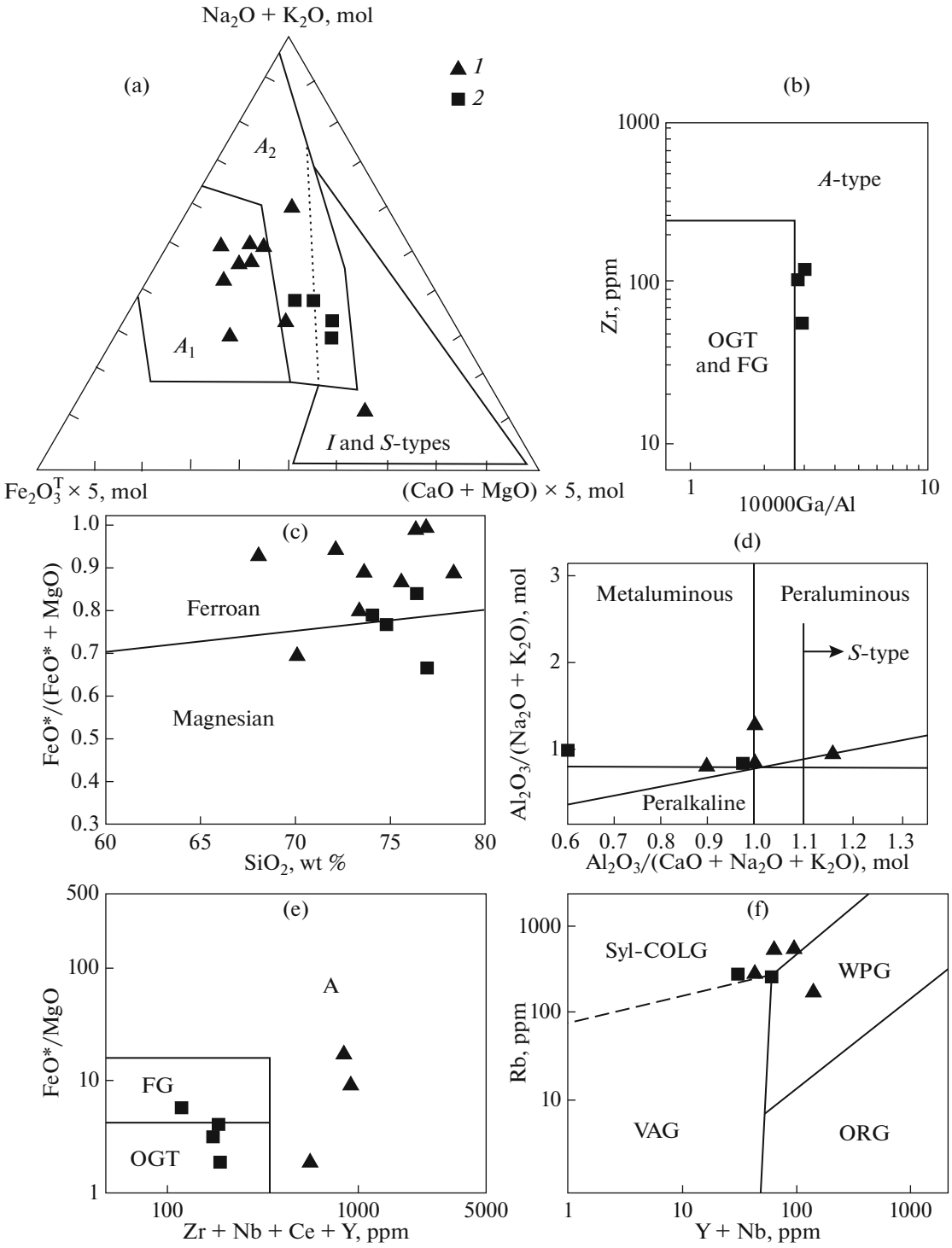

Fig. 3. Geochemical discriminant diagrams. (a) Diagram ($Na_2O + K_2O$)–$Fe_2O_3 \times 5$–($CaO + MgO$) × 5, mol % [9], (A_1) field of siliceous within-plate rocks: oceanic islands and continental rifts; (A_2) felsic magmatic associations of intra- and marginal-continental rifts (compositions are recalculated to dry residue and reduced to 100%); (b) diagram Zr–10000Ga/Al [44], OGT and FG are unfractionated and fractionated granitoids of I and S-types, (A) *A*-type granitoids; (c) diagram SiO_2–FeO*/(FeO* + MgO) [33]; (d) A/NK ($Al_2O_3/(Na_2O + K_2O)$)–A/CNK ($Al_2O_3/(CaO + Na_2O + K_2O)$, mol %) [38]; (e) diagram (Zr + Nb + Ce + Y)–FeO*/MgO [44], OGT fields are nonfractionationed granitoids of *I*- and *S*-types, (FG) fractionated granitoids of *I*-type, (A) *A*-type granitoids; (f) diagram (Y + Nb)–Rb [39], compositional fields: (ORG) ocean ridge granites, (VAG) volcanic arc granites, (Syn-COLG) syn-collisional granites, (WPG) within-plate granites. Granitoids of the Altakhta Complex: (*1*) first phase; (*2*) second phase.

can be related to the plagioclase fractionation (Fig. 4a). The REE content and distribution pattern in the rocks show their moderate differentiation with insignificant LREE predominance over HREE ($(La/Yb)_N$ = from 1.3 to 6.9). Primitive mantle-normalized mutielement patterns of granitoids of the second phase (Fig. 4b) show trace-element fractionation, strong HREE depletion, deep Eu-, Ba-, Ti-, Sr-anomalies, selective P and Zr depletion, and positive Rb, Th, and U anomalies, which is typical of "magmatic rocks of the *A*-geochemical type" [9].

The primitive-mantle and average continental crust-normalized trace element patterns (Figs. 4b, 4c) show clear enrichment of the rocks of the first phase compared to the granites of the second phase in HFSE, REE (103–284 ppm), Rb (to 480 ppm), Th (21–89 ppm), and U (6–34 ppm) against depletion in Ba (up to 600 ppm), Ti, Sr, Ni, Co, and Cr (Table 1). In general, the contents of lithophile elements in the rocks of the second phase correspond to that of the continental crust [43], except for clear enrichment in Th (up to 29 ppm), U (5.5 ppm), Rb (up to 207 ppm) and K, insignificant enrichment in Nb (16–21 ppm), Ta (1.3–1.8 ppm) and, in contrast, a clear depletion in Ba (13–30 ppm), Sr (41–58 ppm), and Ti (297–769 ppm) (Table 1, Fig. 4c). Based on the mineralogical and geochemical features, the rocks of the first phase are sufficiently close to the A_1-type granites, while the second phase are close to $A_2 + I$-type granites [32, 44]. Petrochemically (in the K/Rb–Rb and Sr–Rb/Sr diagrams [22]), the studied granitoids fall in the fields of rocks of crustal and crustal–mantle genesis.

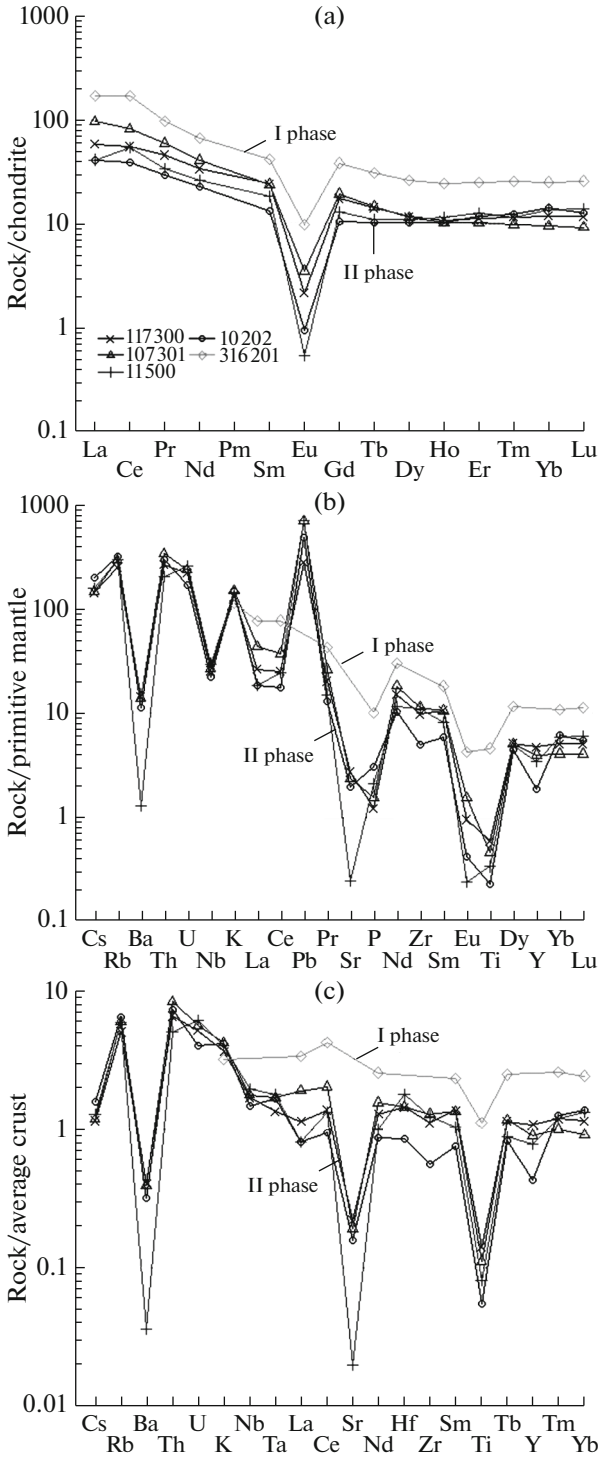

Fig. 4. Trace and rare-earth element patterns in the rocks of the Altakhta Complex, eastern Bureya massif. Hereinafter, sample numbers correspond to those in Table 1. Trace and rare-earth elements were normalized to chondrite (a) [31], primitive mantle (PM) (b) [42], and average crust (c) [43].

GEOCHRONOLOGICAL U–Pb STUDIES

Sample 316201 (sample 5 in Fig. 2; 131°43′20″ N, 50°56′00″ E). Zircons are mainly represented by light pink translucent short-prismatic, bipyramidal crystals and their fragments (Fig. 5, I). The crystal size varies from 100 to 400 μm; the elongation coefficient (K_{el}) is 1.3–4.0. The cathodoluminescence image (CL) shows sectorial magmatic zoning. The U content varies from 337 to 741 ppm, the Th content varies from 148 to 364 ppm, and Th/U ratio varies from 0.37 to 0.73 (Table 3), which is typical of magmatic zircon. Ten concordant points yield an age of 235.3 ± 2.9 Ma, MSWD = 0.38 (Fig. 6). This suggests that obtained age corresponds to the crystallization age of quartz syenites of the first phase of the Altakhta Complex.

Sample 107701 (sample 2 in Fig. 2; 131°58′30″ N, 50°47′50″ E). Zircon is represented by transparent and translucent bipyramidal prismatic pale yellow and pale brown grains of zircon habit. Their inner structure is characterized by coarse magmatic zoning and the presence of inclusions of other mineral phases. The crystal size varies from 100 to 450 μm, K_{el}, 1.4–4.0 (Fig. 5, II). In CL, the transparent and translucent zircons consist of darker inner part and lighter zoned shell. The U content in the zircon grains varies from 462 to 1221 ppm, Th, varies from 166 to 1427 ppm, and

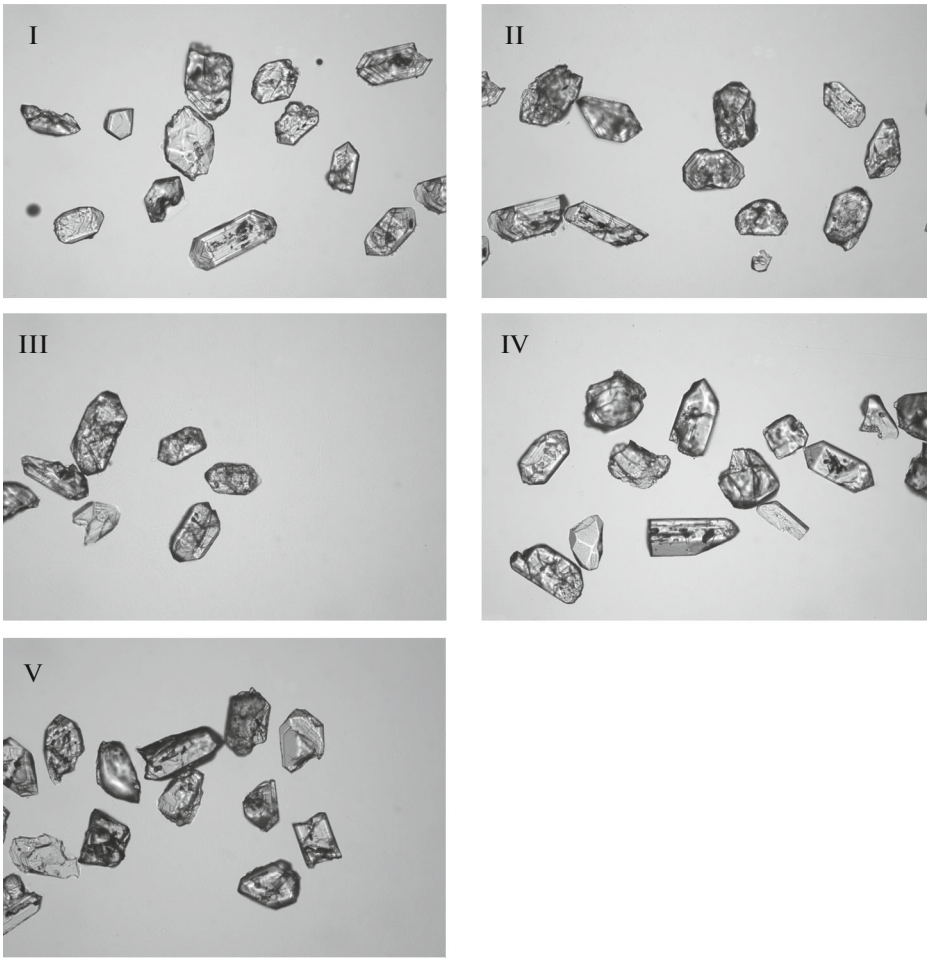

Fig. 5. Microimages of zircon crystals (cathodoluminescence regime). Number of analyzed points are the same as in Tables 3–6.

the Th/U ratio varies from 0.37 to 1.21 (Table 3), which is typical of zircon of magmatic genesis. Concordant age determined from nine points is 226.3 ± 2.9 Ma, MSWD = 2.9 (Fig. 6). This age could be considered as the crystallization age of subalkaline granites of the second phase.

Sample 117300 (sample 1 in Fig. 2; 131°59′25″ N, 50°50′35′′ E). Accessory zircon forms translucent bipyramidal prismatic crystals of hyacinth habit and their fragments of a pale brown color (Fig. 5, III). The crystal size varies from 100 to 400 μm; K_{el} = 1.4–3.5. CL shows a sectorial coarse magmatic zoning. The U content varies from 525 to 2935 ppm, Th , from 434 to 2258 ppm, and Th/U ratio, from 0.50 to 0.95 (Table 4). The high U and Th contents likely reflect the influence of metasomatic processes. Zircon dates are characterized by highly discordant values, which, however, define a clear discordia with sufficiently reliable events. In compliance with the magmatic morphology of the zircons, the concordant age value of 225.7 ± 0.7 Ma (MSWD = 1.3) derived from eight points (Fig. 6) can be interpreted as the estimated age of zircon crystallization and respectively, the age of the subalkaline granites of the second phase.

This sample contains two small pale brown zircon crystals from 140 to 175 μm, K_{el} is 2.0–2.2 (Table 4). The U and Th contents are 265–405 and 74–177 ppm, respectively, and Th/U ratio is 0.29–0.45. In terms of these parameters, they differ from zircons of the first group. The morphological features of these crystals and concentrations of radiogenic elements are typical of zircons of magmatic genesis. Points 6.1 and 7.1 of sample 117300 (Table 4) characterize inherited domains of the crystals and reflect the protolith age. Ages of 443.7 ± 2.9 and 465.5 ± 2.5 Ma obtained on two analyses are close to the formation age of the Ordovician granites of the Sularin Complex [1, 46].

Sample 11500 (sample 3 in Fig. 2; 131°58′15″ N, 50°48′30″ E). Zircons are represented by pinkish brown and brown color short-prismatic, sometimes fractured zircons of zircon habit and their fragments (Fig. 5, IV). They contain small brownish and black inclusions. CL reveals a coarse magmatic zoning. The crystals are 110–450 μm in size, K_{el} is 1.2–3.5. The U

Table 3. Analytical data on zircons from quartz syenites and subalkaline granites of the Altakhta Complex, eastern Bureya massif (samples 316201, 107701)

Point no.	% $^{206}Pb_c$	U, ppm	Th, ppm	$\frac{^{232}Th}{^{206}Pb^*}$	$^{206}Pb^*$, ppm	(1) Age $\frac{^{206}Pb}{^{238}U}$	(2) Age $\frac{^{206}Pb}{^{238}U}$	(1) Age $\frac{^{207}Pb}{^{206}Pb}$	D, %	$\frac{^{238}U}{^{206}Pb}$	±, %	(1) $\frac{^{207}Pb}{^{206}Pb}$	±, %	(1) $\frac{^{207}Pb^*}{^{235}U}$	±, %	(1) $\frac{^{206}Pb^*}{^{238}U}$	±, %	Rho
Quartz syenites of the first phase, sample 316201																		
1.1	0.00	397	148	0.38	13.0	241.4 ± 4.8	240.8 ± 4.8	337 ± 93	40	26.21	2.0	0.0532	4.1	0.280	4.6	0.03816	2.0	0.442
2.1	0.00	337	148	0.45	10.7	234.6 ± 5.1	233.9 ± 5.2	334 ± 100	43	26.99	2.2	0.0531	4.4	0.271	4.9	0.03706	2.2	0.448
3.1	0.50	513	194	0.39	16.8	239.3 ± 4.6	238.9 ± 4.6	307 ± 130	28	26.33	1.9	0.0565	3.4	0.274	6.1	0.03782	2.0	0.322
4.1	0.49	513	364	0.73	16.4	235.2 ± 4.6	234.8 ± 4.6	291 ± 130	24	26.78	2.0	0.0560	3.6	0.267	6.1	0.03716	2.0	0.323
5.1	0.25	520	226	0.45	16.6	234.5 ± 4.5	234.5 ± 4.5	231 ± 100	−2	26.92	1.9	0.0528	3.6	0.259	4.8	0.03705	2.0	0.407
6.1	0.24	553	217	0.41	17.5	232.7 ± 4.4	232.8 ± 4.5	220 ± 99	−5	27.13	1.9	0.0525	3.5	0.256	4.7	0.03676	1.9	0.414
7.1	0.63	411	161	0.41	13.3	236.7 ± 4.7	236.7 ± 4.8	239 ± 160	1	26.56	2.0	0.0560	3.9	0.263	7.2	0.03740	2.0	0.283
8.1	0.00	741	309	0.43	23.3	231.4 ± 4.5	231.3 ± 4.5	244 ± 69	5	27.36	2.0	0.0511	3.0	0.257	3.6	0.03655	2.0	0.547
9.1	0.47	523	257	0.51	16.9	236.0 ± 4.6	237.3 ± 4.6	158 ± 140	−33	26.60	2.0	0.0530	3.6	0.254	6.3	0.03741	2.0	0.316
10.1	0.33	681	243	0.37	21.5	232.0 ± 4.4	232.2 ± 4.4	207 ± 110	−11	27.20	1.9	0.0529	3.2	0.254	4.9	0.03664	1.9	0.389
Porphyritic subalkaline granites of the second phase, sample 107701																		
1.1	0.00	523	373	0.74	15.9	223.8 ± 4.3	224.0 ± 4.4	197 ± 56	−12	28.31	2.0	0.0501	2.4	0.244	3.1	0.03533	2.0	0.628
2.1	0.00	576	338	0.61	17.6	225.2 ± 4.3	225.0 ± 4.4	262 ± 52	16	28.13	2.0	0.0515	2.3	0.2523	3.0	0.03555	2.0	0.654
3.1	0.27	740	316	0.44	22.8	226.2 ± 4.3	226.5 ± 4.4	177 ± 78	−22	27.93	1.9	0.0518	2.1	0.2443	3.9	0.03571	1.9	0.504
4.1	0.00	461	166	0.37	14.2	227.0 ± 4.4	226.9 ± 4.5	233 ± 61	2	27.91	2.0	0.0508	2.7	0.2511	3.3	0.03584	2.0	0.600
5.1	0.00	736	674	0.95	22.7	227.4 ± 4.3	227.6 ± 4.4	202 ± 49	−11	27.85	1.9	0.0502	2.1	0.2483	2.9	0.03591	1.9	0.681
6.1	0.19	1139	901	0.82	35.1	226.7 ± 4.3	226.6 ± 4.3	237 ± 56	4	27.89	1.9	0.0524	1.7	0.2512	3.1	0.03578	1.9	0.623
7.1	0.26	711	761	1.02	23.7	224.9 ± 4.3	226.1 ± 4.3	204 ± 75	−10	27.96	1.9	0.0523	2.0	0.2468	3.8	0.03567	1.9	0.518
8.1	0.00	606	339	0.58	18.5	224.9 ± 4.3	224.4 ± 4.4	303 ± 52	35	28.17	2.0	0.0524	2.3	0.2565	3.0	0.03555	2.0	0.653
9.1	0.00	1221	1427	1.21	37.4	225.5 ± 4.3	225.7 ± 4.3	201 ± 39	−11	28.09	1.9	0.0501	1.7	0.2461	2.5	0.03560	1.9	0.755
10.1	3.24	974	515	0.55	29.5	216.2 ± 4.3	215.9 ± 4.1	279 ± 190	29	28.36	1.9	0.0777	1.5	0.2440	8.5	0.03410	2.0	0.237

Hereinafter, (Pb_c) common lead, (Pb*) radiogenic lead. Errors relative to the calibration standard is 0.65% (sample 316201), 0.53% (sample 107701), 0.23% (sample 117300), 0.45% (sample 11500), 0.41% (sample 10202) (indicated above error is not included, but is required for data comparison). Errors in age determination are given at 1σ level, while that of isotope ratios, at 2σ. (1) Correction for unradiogenic lead based on measured Pb^{204}. (2) Total Pb with correction assuming age $^{206}Pb/^{238}U$–$^{207}Pb/^{235}U$ concordance. (D) degree of discordance. For sampling localities, see Fig. 2.

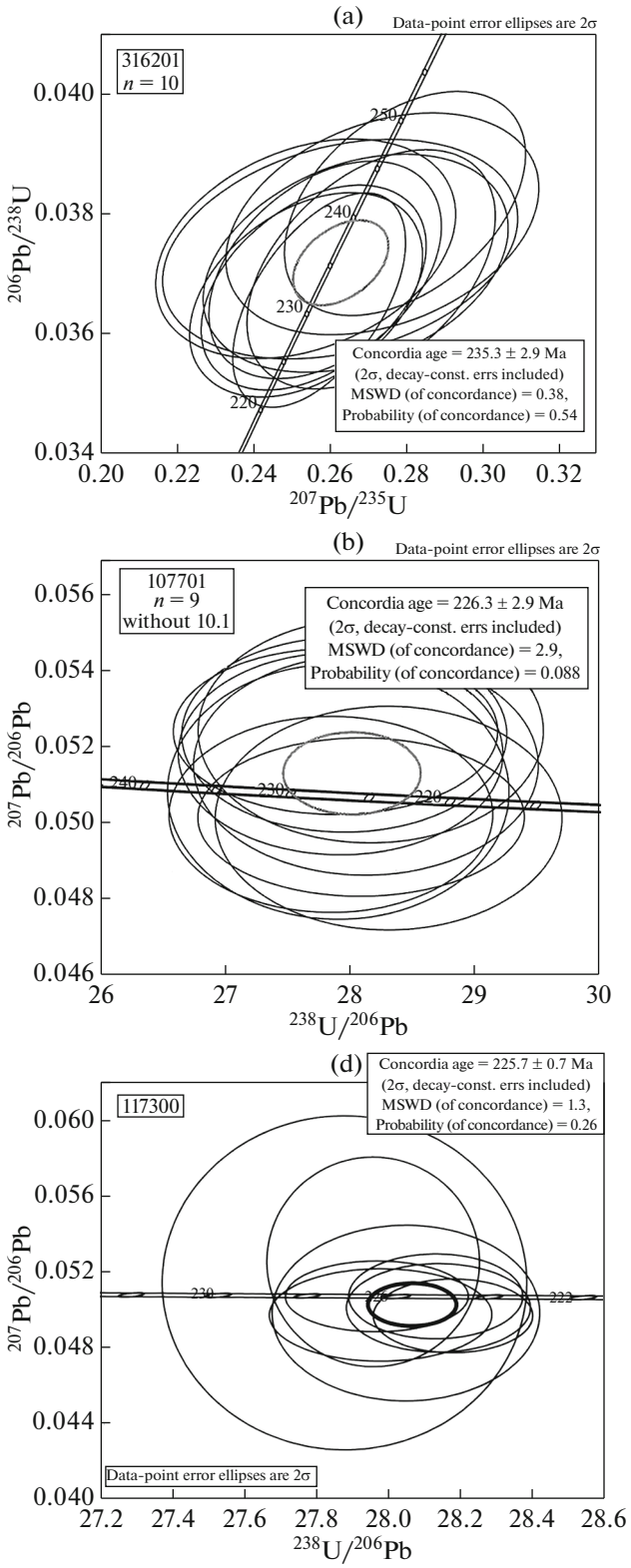

Fig. 6. Concordia diagram for zircons from granitoids of the first (a) and second (b, c) phases of the Altakhta Complex.

and Th contents vary from 734 to 2716 ppm and from 338 to 1684 ppm, Th/U = 0.43–1.10 (Table 5). The high U and Th contents likely reflect the influence of autometasomatic processes. The concordant age derived from nine analyses, excluding the youngest and oldest ages, is 224.9 ± 2.5 Ma (MSWD = 1.19, probability 0.081). These zircon grains yield highly discordant ages, but discordia are well-defined and the revealed events are sufficiently reliable. Given these facts, the value of 224.9 ± 2.5 Ma can be accepted as the crystallization age of the leucogranites of the second phase, which was intruded by Late Triassic subvolcanic trachyrhyolites of the Talovsky Complex (218.1 ± 2.8 Ma, U–Pb SHRIMP-II, zircon) at observation point no. 11500 [1, 46].

Sample 10202 (sample 4 in Fig. 2; 131°47′10″ N, 50°43′30″ E). Zircons are represented by translucent and transparent yellowish and brownish short prismatic crystals (Fig. 5, V). Single grains comprise inclusions of other mineral phases of darker color. In appearance, the grains are homogenous. CL imaging displays zones of coarse sectorial magmatic zoning. Results of U–Pb analyses are shown in Table 6. Analytical points are concordant within an error ellipse, but one point yields a slightly rejuvenated age. The concordant age obtained from 10 points is 224.9 ± 2.4 (MSWD = 1.09, probability 0.33) [44]. The obtained value can be accepted as the formation age of leucogranites of the second phase, which in this area (observation point no. 10202) intrude the Late Permian–Early Triassic granodiorites of the third phase of the Tyrma–Bureya Complex [1].

DISCUSSION

The presented geochronological data indicate that the studied granitoids from the intrusions in the middle reaches of the Bureya River have Late Triassic age of 235.3 ± 2.9–224.9 ± 2.4 Ma, rather than Permian, Permotriassic, and Jurassic ages as suggested earlier [4, 13, 15, 17]. This age of the Altakhta granitoids is confirmed by the fact that they cut across granitoids of the Tyrma–Bureya Complex (254.2 ± 2.5–246.6 ± 3.0 Ma), and, in turn, are intersected by trachyrhyolite dikes (218.1 ± 2.8 Ma) of the Talovsky Complex and are intruded by quartz diorites (206.5 ± 2.5 Ma) and leucogranites (199.0 ± 4.0 Ma) of the Kharin Complex (U–Pb SHRIMP-II, zircon, [1, 10]). These data were used to distinguish them as an independent Late Triassic complex, for which we propose the former traditional name, that is, the Altakhta Complex.

The generalization of geological and geochronological (Tables 3–6) results of our studies allowed us to distinguish two intrusive phases in the formation of intrusions of the Altakhta syenite–leucogranite complex: *the first phase (235–230 Ma)* is made up of syenites, quartz syenites, quartz monzonites, granosyenites, alkaline granites, and alkaline granosyenites; *the second phase (226–224 Ma)* is represented by subalkaline leucogranites, granites, leucogranite porphyries, dikes of granite porphyry and subalkaline leu-

Table 4. Analytical data on zircons from subalkaline granites of the second phase of the Altakhta Complex, sample 117300

Point no.	% $^{206}Pb_c$	U, ppm	Th, ppm	$\frac{^{232}Th}{^{238}U}$	$^{206}Pb^*$, ppm	(2) Age $\frac{^{206}Pb^*}{^{238}U}$	(1) $\frac{^{238}U}{^{206}Pb^*}$	±, %	(1) $\frac{^{207}Pb^*}{^{206}Pb^*}$	±, %	(1) $\frac{^{207}Pb^*}{^{235}U}$	±, %	(1) $\frac{^{206}Pb^*}{^{238}U}$	±, %	Rho
1.1	0.10	2413	1169	0.50	74.2	226.42 ± 0.8	27.9	0.37	0.0506	1.5	0.249	1.6	0.03575	0.37	0.232
3.1	0.32	2935	2258	0.80	89.6	225.16 ± 0.78	28.13	0.3335	0.0506	1.8	0.2483	1.8	0.03554	0.35	0.193
4.1	0.10	1035	542	0.54	31.8	226.6 ± 1.0	27.98	0.45	0.0497	2.0	0.245	2.1	0.03574	0.45	0.213
5.1	1.10	525	481	0.95	16.4	227 ± 1.4	27.88	0.74	0.0514	7.0	0.254	7.1	0.03586	0.74	0.105
8.1	0.16	2453	1292	0.54	74.9	225.08 ± 0.71	28.18	0.32	0.0496	1.6	0.2429	1.6	0.03549	0.32	0.197
9.1	0.44	775	434	0.58	23.9	226.1 ± 1.2	28.05	0.54	0.0498	3.8	0.2448	3.8	0.03565	0.54	0.141
9.1RE	2.11	2608	1378	0.55	81.8	226 ± 0.84	27.96	0.43	0.0525	4.3	0.259	4.4	0.03575	0.43	0.099
10.1	0.18	2615	1503	0.59	80.0	225.24 ± 0.8	28.14	0.37	0.0501	1.9	0.2453	1.9	0.03553	0.37	0.189
2.1	1.07	116	95	0.85	3.14	197.1 ± 2.7	32.03	1.40	0.0544	11.0	0.234	11.0	0.03122	1.40	0.134
6.1	0.81	265	74	0.29	16.3	443.7 ± 2.9	14.12	0.75	0.0512	6.2	0.505	6.2	0.07082	0.75	0.120
7.1	0.09	405	177	0.45	26.1	465 ± 2.5	13.33	0.54	0.0579	2.2	0.599	2.2	0.07502	0.54	0.239

cogranites; and aplitic, aplite-like, and pegmatite veins.

Petrochemically, the Altakhta granitoids are moderate and high-Al K–Na rocks of moderate and normal alkalinity with elevated K_2O contents. Their geochemical peculiarity is the total REE depletion: REE contents vary from 161 to 282 ppm in rocks of the first phase, from 77 to 146 ppm in rocks of the second phase, which is lower than those of within-plate granites, but is close to those of collisional and subduction granitoids [5]. The REE distribution pattern in them is almost identical to that of the average crust. Geochemically, the granitoids of the second phase differ from magmatic rocks of the first phase in the lowered Fe and Ti contents, lower contents of total REE, typomorphic HFSE and U, Th, Ba, and Rb, and elevated concentrations of "transition" (Ni, Co, and Cr) elements (Tables 1, 2, Fig. 4).

Syenites, granosyenites, alkaline granites, and alkaline granosyenites of the first phase (Tables 1, 2) are ferroan rocks ascribed to *A*-type granitoids according to Frost classification [33] and fall in the field of A_1-type granitoids in the diagram by Grebennikov [9] (Fig. 3a). This is supported by their position in the classification diagram (Fig. 3e) [44] and the similarity of trace element patterns to those of within-plate granitoids [5]. In terms of HREE and Eu contents, they are close to the subduction and collisional granites. They are characterized by the high alkali contents and extremely low, frequently nearly zero MgO and CaO concentrations, which are expressed in their high- and ultra-potassium agpaitic ferroan compositions and elevated Ti contents (Tables 1, 2) at high FeO*/MgO (2–20), which could indicate the affiliation of rocks of the first phase to the tholeiitic series. Their Fe mole fraction at extremely low Mg contents is a characteristic petrochemical parameter in distinguishing *A*-type granites [9]. In general, these features are consistent with mineralogical characteristics of the rocks of the first phase, in particular, with the presence of aegirine, riebeckite, bluish green hornblende, arfvedsonite, aegirine-augite, albite, and Ti-magnetite.

The granites of the second phase have slightly different chemical composition (Table 1), which is clearly seen in the classification (Fig. 3e, [44]) and geochemical discriminant (Fig. 3a, [9]) diagrams. They are characterized by moderate alkali contents, elevated concentrations of MgO, CaO, and FeO^{tot}, and low TiO_2 (Table 1). They are classified as metaluminous and slightly peraluminous high-K granites. Their mineral composition is characterized by the presence of biotite, alkaline (bluish-green) hornblende, and magnetite. Chemically, the studied rocks correspond to nonfractionated and fractionaled granites of *I*- and *S*-types (Fig. 3e), which in the Zr–10000 × Ga/Al diagram (Fig. 3b) fall in the field of *A*-type granites and can be characterized as magmatic rocks of the *A*-geochemical type [44]. The position of the composition data points of the second phase in the fields of granitoids of different geodynamic settings in the Whalen diagram (Figs. 3b, 3e), as well as in the A_2 and A_2+ *I* & *S*-type fields in the Grebennikov diagram (Fig. 3a) is caused by the fact that they bear traces of interaction of crustal magmas with enriched material of sublithospheric mantle [9]. On the one hand, the granites of the second phase are clearly enriched in such elements as Rb, K, Th, U, and Pb at relative depletion in Nb, Ta, Y, HREE, Sr, Ba, Ti, and P, which is typical of magmatic rocks of collisional zones. On the other hand, a significant accumulation of U, Th, Rb and removal of Sr, P, Ba, and Ti are caused by significant contamination of mantle melts with felsic crustal material (A_2). The depletion of granites in Nb, Ta, Ti, and P makes them similar with sub-

Table 5. Analytical data on zircons from porphyritic subalkaline leucogranites of the second phase of the Altakhta Complex, sample 11500.

Point no.	% $^{206}Pb_c$	ppm U	ppm Th	$^{232}Th/^{238}U$	ppm $^{206}Pb^*$	(1) $^{206}Pb/^{238}U$ Age	(2) $^{206}Pb/^{238}U$ Age	Total $^{238}U/^{206}Pb$	±%	Total $^{207}Pb/^{206}Pb$	±%	(1) $^{238}U/^{206}Pb^*$	± %	(1) $^{207}Pb^*/^{206}Pb^*$	±%	(1) $^{207}Pb^*/^{235}U$	±%	(1) $^{206}Pb^*/^{238}U$	± %	Rho
1.1	0.05	3953	2136	0.56	107.0	199.1 ± 3	174.7 ± 2.7	31.86	1.5	0.14957	0.57	31.87	1.5	0.1492	0.62	0.645	1.6	0.03138	1.5	0.925
4.1	0.13	2572	1219	0.49	78.0	223.4 ± 3.3	221.4 ± 3.3	28.32	1.5	0.05909	0.97	28.36	1.5	0.05805	1.1	0.2822	1.9	0.03526	1.5	0.799
8.1	0.14	2568	1485	0.60	78.0	223.7 ± 3.3	223.7 ± 3.4	28.28	1.5	0.05172	1.0	28.32	1.5	0.05058	1.2	0.2463	1.9	0.03531	1.5	0.782
11.1	0.31	734	338	0.48	22.4	224.0 ± 3.5	224.9 ± 3.6	28.19	1.6	0.04989	2.0	28.28	1.6	0.0474	2.8	0.231	3.2	0.03536	1.6	0.496
3.1	0.12	1617	1208	0.77	49.3	224.8 ± 3.4	225.0 ± 3.4	28.15	1.5	0.05068	1.3	28.18	1.5	0.0497	1.6	0.2432	2.2	0.03548	1.5	0.697
2.1	0.08	2056	1684	0.85	63.3	226.9 ± 3.4	227.1 ± 3.4	27.9	1.5	0.05046	1.2	27.92	1.5	0.04981	1.4	0.246	2.1	0.03582	1.5	0.727
6.1	0.03	1504	1604	1.10	46.8	229.1 ± 3.9	229.4 ± 3.9	27.63	1.7	0.05002	1.4	27.64	1.7	0.04982	1.4	0.2485	2.3	0.03618	1.7	0.766
9.1	0.08	1772	734	0.43	55.2	229.3 ± 3.5	223.4 ± 3.4	27.59	1.5	0.07210	2.1	27.62	1.5	0.0715	2.2	0.357	2.7	0.03621	1.5	0.570
5.1	0.06	2766	1533	0.57	87.3	232.4 ± 3.5	232.4 ± 3.5	27.23	1.5	0.05126	1.5	27.24	1.5	0.05081	1.5	0.2572	2.1	0.03671	1.5	0.706
7.1	0.10	1627	1470	0.93	51.7	234.0 ± 3.5	234.4 ± 3.6	27.02	1.5	0.05042	1.6	27.05	1.5	0.04964	1.8	0.253	2.4	0.03697	1.5	0.645
10.1	0.04	228	124	0.56	67.7	1914 ± 2.6	1918 ± 30	2.892	1.6	0.11548	0.79	2.893	1.6	0.11515	0.81	5.487	1.8	0.3456	1.6	0.888

Table 6. Analytical data on zircons from subalkaline leucogranites of the second phase of the Altakhta Complex, sample 10202

Point no.	% $^{206}Pb_c$	ppm U	ppm Th	$^{232}Th/^{238}U$	ppm $^{206}Pb^*$	(1) $^{206}Pb/^{238}U$ Ma	(2) $^{206}Pb/^{238}U$ Ma	Total $^{238}U/^{206}Pb$	± %	Total $^{207}Pb/^{206}Pb$	± %	(1) $^{238}U/^{206}Pb^*$	± %	(1) $^{207}Pb^*/^{206}Pb^*$	± %	(1) $^{207}Pb^*/^{235}U$	± %	(1) $^{206}Pb^*/^{238}U$	± %	Rho
1.1	0.14	3031	2024	0.69	90.6	220.2 ± 3.3	215.5 ± 3.2	28.74	1.5	0.06869	0.85	28.78	1.5	0.06763	1.0	0.3240	1.8	0.03475	1.5	0.832
2.1	0.28	517	221	0.44	17.3	245.0 ± 3.9	245.5 ± 4.0	25.75	1.6	0.0514	2.2	25.82	1.6	0.0492	2.8	0.2628	3.2	0.03873	1.6	0.505
3.1	0.66	318	141	0.46	9.72	223.7 ± 3.7	225.9 ± 3.8	28.13	1.7	0.0482	3.1	28.31	1.7	0.0429	5.6	0.2090	5.9	0.03532	1.7	0.290
4.1	0.61	337	143	0.44	10.4	225.5 ± 3.7	227.0 ± 3.8	27.91	1.7	0.0504	2.9	28.09	1.7	0.0454	5.5	0.2231	5.7	0.03561	1.7	0.293
5.1	0.58	358	185	0.53	10.8	220.9 ± 3.8	222.0 ± 3.8	28.52	1.7	0.0513	2.9	28.68	1.7	0.0466	5.2	0.2241	5.4	0.03486	1.7	0.319
6.1	0.19	467	389	0.86	14.1	222.3 ± 3.5	222.3 ± 3.6	28.45	1.6	0.0522	2.4	28.50	1.6	0.0506	3.1	0.2448	3.5	0.03508	1.6	0.467
7.1	0.09	665	214	0.33	20.3	225.2 ± 3.5	225.5 ± 3.5	28.10	1.6	0.0504	2.1	28.13	1.6	0.0497	2.3	0.2436	2.8	0.03555	1.6	0.566
8.1	0.11	924	1049	1.17	28.0	223.5 ± 3.4	223.6 ± 3.4	28.31	1.5	0.0512	2.0	28.35	1.6	0.0503	2.2	0.2447	2.7	0.03528	1.6	0.573
9.1	0.03	1883	931	0.51	57.7	225.8 ± 3.4	225.6 ± 3.4	28.05	1.5	0.05143	1.2	28.06	1.5	0.0512	1.3	0.2516	2	0.03564	1.5	0.762
10.1	0.44	609	424	0.72	18.6	224.5 ± 3.5	225.1 ± 3.6	28.09	1.6	0.0522	2.2	28.21	1.6	0.0487	3.4	0.2381	3.7	0.03544	1.6	0.429
11.1	0.12	538	250	0.48	16.4	224.9 ± 3.6	225.2 ± 3.6	28.13	1.6	0.0504	2.4	28.17	1.6	0.0495	2.6	0.2421	3.1	0.03550	1.6	0.522

duction zone rocks and suggests the involvement of asthenospheirc diapir and its fluids in the parental melts. Moreover, their spidergrams (Figs. 4b, 4c) show negative Ba- and Sr-anomalies and positive Rb anomaly, which is not typical of subduction granites [41]. In terms of REE and trace element contents, they occupy an intermediate position between subduction and collisional granitoids [5]. A combination of contrasting within-plate and suprasubduction characteristics and the presence of *A*, *I*, and *S*-types of the same age in the Altakhta granites mark their formation on a transform continental margin [8, 26–28]. The accumulation of Th, U, Rb, Pb and depletion in Sr, P, Ba, and Ti in the granites are likely related to heating and partial melting of continental crust under the influence of heat and mantle material, as shown in [9, 27].

Two stages of the Altakhta granitoid magmatism separated by an insignificant gap of 5–10 Ma are established in the eastern part of the BM. The first stage produced high and ultrahigh-K, agpaitic, high-Fe and high-Ti A_1-type granitoids (235–230 Ma). The second stage was responsible for the formation of metaluminous and slightly peraluminous, high-K magnesian–ferroan and low-Ti granites of the A_2 and A_2+ *I* & S-types (226–224 Ma), which geochemically are close to the magmatic rocks of the first phase, thus suggesting their close magma generation source. The difference between the compositions of the granitoids of the first (A_1-type) and second (A_2 and A_2+ *I* & S-types) phases is expressed in decreasing mantle component in the granites of the final phase and controlled by the interaction of deep-seated (mantle) melts reaching middle crustal levels with crustal material and on structural conditions of their penetration [9].

Thus, the chemical evolution of the Altakhta granitoids indicates a change of geodynamic setting in the eastern part of the BM from (orthogonal) movement of plates near a convergent boundary (subduction) to strike-slip movements relative each other, which was determined by Khanchuk [26–28] as a transform continental margin.

CONCLUSIONS

A stage of granitoid magmatism between 235.3 ± 2.9 and 224.9 ± 2.4 Ma was distinguished in the Early Mesozoic history of the eastern BM of the CAFB. Data presented in the paper are used to recognize an independent Late Triassic syenite–leucogranite complex, for which we propose to return the former traditional name of the Altakhta Complex. It was established that the complex consists of two phases.

The first phase (235–230 Ma) produced syenites, quartz monzonites, quartz syenites, granosyenites, alkaline granites, and alkaline granosyenites. They are classified as high- and ultrahigh-K agpaitic, ferroan and high-Ti A_1-type granites. They are similar to the A_1-type within-plate granitoids in geochemistry and resemble collisional and subduction granites in terms of HREE and Eu concentrations. The magmatic rocks of the first phase were likely formed in a within-plate setting near divergent boundaries of the northeastern BM (lithospheric plate) in a cold intracontinental rift, where pull-apart structures provided a penetration of deep-seated melts or mantle matter. The second phase (226–224 Ma) involved the formation of subalkaline leucogranites and granites, leucogranite porphyry, dikes of granite porphyry, as well as aplite and pegmatite veins. These rocks correspond to the metaluminous and weakly peraluminous, high-K, magnesian–ferroan, low-Ti granites of A_1 and A_2+ *I* & *S*-types. Chemically, they are ascribed to the nonfractionated and fractionated *I*- and *S*-type granitoids, which correspond to A-type granites in terms of high Ga/Al ratios and can be characterized as *A*-geochemical type of magmatic rocks [44]. They bear traces of interaction of crustal magmas with enriched material of sublithospheric mantle and were formed in a different setting than the granitoids of the first phase. The accumulation of Th, U, Rb, and Pb and removal of Sr, P, Ba, and Ti in the granites of second phase could be related to heating and partial melting of continental crust at intense influx of heat and mantle material, as was shown by Khanchuk [27], during formation of parent melts under the influence of asthenospheric diapir and assisted fluids. The difference in the composition between granitoids of the first (A_1-type) and second (A_2 and A_2+ *I* & *S*-types) phases is expressed in a decreasing mantle contribution with time, which is controlled by the interaction of mantle melts that reach the middle continental crust with crustal material (assimilation) and structural conditions of their penetration [9].

The available data suggest that the period of 235–224 Ma (Late Triassic) in the eastern BM was marked by a change of geodynamic setting from convergent movement of plates (subduction) to their strike-slip displacement relative each other (transform continental margins).

ACKNOWLEDGMENTS

We are grateful to Academician A.I. Khanchuk and A.V. Grebennikov for constructive comments and fruitful consultation and recommendation, which significantly improved our manuscript.

FUNDING

The studies were carried out in the framework of the State Task of the Kosygin Institute of Tectonics and Geodynamics of the Far East Branch of the Russian Academy of Sciences and supported by the Federal Agency on the Nature Management (State Contract on the Preparation of Gosgeolkarta-200, sheet M-52-XII).

REFERENCES

1. V. N. Arapov and S. A. Amelin, *State Geological Map of the Russian Federation. 1 : 200000. 2nd Ed. Sheet N-52-XII: Explanatory Note*, Ed. by G.V. Roganov (Kartfabrika VSEGEI, St. Petersburg, 2018) [in Russian].
2. *Bureya Sedimentary Basin: Geological-Geophysical Characteristics, Geodynamics, and Fuel–Energetic Resources*, Ed. by G.L. Kirilova (Dal'nauka, Vladivostok, 2012) [in Russian].
3. V. V. Vasil'eva, *State Geological Map of the SSSR. 1 : 200000. Khingan–Bureya Series. Sheet M-52-18: Explanatory Note* (Gosgeoltekhizdat, Moscow, 1962) [in Russian].
4. A. F. Vas'kin, V. A. Dymovich, A. F. Atroshenko, V. B. Grigor'ev, V. N. Zelepugin, E. S. Opalikhina, L. A. Sharov, and Yu. L. Leont'eva, *State Geological Map of the Russian Federation (3rd Generation). 1 : 1000000. Far East Series. Sheet M-53 Khabarovsk: Explanatory Note*, Ed. by A. F. Vas'kin (Kartfabrika VSEGEI, St. Petersburg, 2009) [in Russian].
5. S. D. Velikoslavinskii, "Geochemical classification of silicic igneous rocks of major geodynamic environments," Petrology **11** (4), 327–342 (2003).
6. V. G. Gonevchuk, G. A. Gonevchuk, and M. A. Kokorin, "Tin-bearing pegmatites of the Bureya massif," Tikhookean. Geol. **14** (2), 126—133 (1995).
7. V. G. Gonevchuk, *Far East Tin-Bearing Systems: Magmatism and Ore Genesis* (Dal'nauka, Vladivostok, 2002) [in Russian].
8. V. G. Gonevchuk and G. A. Gonevchuk, "Eastern Bureya granitic belt (Triassic)," *Geodynamics, Magmatism, and Metallogeny of East Russia*, Ed. by A. I. Khanchuk (Dal'nauka, Vladivostok, 2006), vol. 1 [in Russian].
9. A. V. Grebennikov, "A-type granites and related rocks: problems of identification, petrogenesis, and classification," Russ Geol. Geophys. **55** (9), 1356–1373 (2014).
10. V. A. Guryanov, E. V. Nigai, Yu. Yu. Yurchenko, S. N. Dobkin, V. N. Arapov, and S. A. Amelin, "Chronology of the granitoid magmatism of the eastern Bureya massif of the Central Asian Fold Belt," *Methods and Geochronological Results of Study of Isotope Geochronological Systems of Minerals and Rocks. 7th Russian Conference on Isotope Geochronology* (IGEM RAN, Moscow, 2018), pp. 105–108 [in Russian].
11. E. M. Zablotskii and A. S. Stukanov, *State Geological Map of the Russian Federation. 1 : 1000000 (New Series). Sheet M52, 53. Blagoveshchensk: Explanatory Note* (Kartfabrika VSEGEI, St. Petersburg, 1996) [in Russian].
12. A. B. Kotov, S. D. Velikoslavinskii, A. A. Sorokin, L. N. Kotova, A. P. Sorokin, A. M. Larin, V. P. Kovach, N. Yu. Zagornaya, and A. V. Kurguzova, "Age of the Amur Group of the Bureya–Jiamusi Superterrane in the Central Asian Fold Belt: Sm-Nd isotope evidence," Dokl. Earth Sci. **428** (5), 1245–1248 (2009).
13. L. I. Krasnyi and Pen Yun'byao, *Geological Map of the Amur Region and Adjacent Territories. 1 : 2500000: Explanatory Note* (Blagoveshchensk–Kharbin, St. Petersburg, 1999) [in Russian].
14. B. I. Lovi, "Intrusive complexes of Lesser Khingan," in *Geological Evolution and Magmatism of Lesser Khingan* (VSEGEI, Leningrad, 1961), pp. 65–122 [in Russian].
15. M. V. Martynyuk, S. A. Ryamov, and V. A. Kondrat'eva, *Explanatory Note to the Scheme of Subdivision and Correlation of Magmatic Complexes of the Khabarovsk Krai and Amur Oblast* (Min.geo. SSSR, DV PGO, TsTP, Khabarovsk, 1990) [in Russian].
16. L. M. Parfenov, N. A. Berzin, A. I. Khanchuk, G. Badarch, V. G. Belichenko, A. I. Bulgatov, S. I. Dril', G. L. Kirilova, M. I. Kuz'min, U. Nokleberg, A. V. Prokop'ev, V. F. Timofeev, O. Tomurtogoo, and H. Jahn, "Model of formation of orogenic belts of Central and Northeastern Asia," Tikhookean. Geol. **22** (6), 7–41 (2003).
17. N. N. Petruk, Yu. R. Volkova, N. M. Shilova, A. V. Myalik, N. I. Shadrina, and A. I. Azarova, *"State Geological Map of the Russian Federation (3rd Generation). 1 : 1000000. Far East Series. Sheet M-52—Blagoveshchensk: Explanatory Note,* Ed. by A. S. Vol'skii (Kartfabrika VSEGEI, St. Petersburg, 2012) [in Russian].
18. V. A. Popeko, "Magmatic formations of the Bureya massif," in *Magmatic Formations of Active Continental Margins* (Nauka, Moscow, 1980), pp. 118–142 [in Russian].
19. V. K. Putintsev, E. M. Zablotskii, and L. M. Kolmak, *Magmatic Formations of the Far East Activated Areas and Their Metallogenic Specialization* (VSEGEI, Leningrad, 1970) [in Russian].
20. Yu. P. Rasskazov, *State Geological Map of the USSR. 1 : 200 000. Khingan–Bureya Series. Sheet M-52-XII* (Gosgeoltekhizdat, Moscow, 1959) [in Russian].
21. A. I. Romashkin, "Geochemical evolution of the granite-gneiss complex of the Bureya massif," Tikhookean. Geol., No. 4, 93–102 (1987).
22. M. G. Rub, N. G. Gladkov, V. A. Pavlov, A. K. Rub, and N. V. Troneva, "Alkaline element and strontium in ore-bearing (Sn, W, Ta) differentiated magmatic associations," Dokl. Akad. Nauk SSSR **268** (6), 1463–1466 (1983).
23. A. A. Sorokin, A. B. Kotov, E. B. Sal'nikova, N. M. Kudryashov, S. D. Velikoslavinskii, S. Z. Yakovleva, A. M. Fedosenko, and Yu. V. Plotkina, "Early Paleozoic granitoids in the Lesser Khingan Terrane, Central Asian Foldbelt: age, geochemistry, and geodynamic interpretations," Petrology **19** (6), 601–617 (2011).
24. A. A. Sorokin, R. O. Ovchinnikov, N. M. Kudryashov, A. B. Kotov, and V. P. Kovach, "Two stages of Neoproterozoic magmatism in the evolution of the Bureya continental massif of the Central Asian Fold Belt," Russ. Geol. Geophys. **58** (10), 1171–1187 (2017).
25. S. R. Taylor and S. M. McLennan, *The Continental Crust: Its Composition and Evolution* (Blackwell Scientific Publ., Oxford, 1985) [in Russian].
26. A. I. Khanchuk, V. V. Golozubov, Yu. A. Martynov, and V. P. Simanenko, "Early Cretaceous and Paleogene transform continental margins (Californian type) of Far East," in *Tectonics of Asia* (GEOS, Moscow, 1997), pp. 240–243 [in Russian].
27. A. I. Khanchuk and V. V. Ivanov, "Meso-Cenozoic geodynamic setting and gold mineralization of the Russian Far East," Geol. Geofiz. **40** (11), 1635–1645 (1999).
28. A. I. Khanchuk, A. V. Grebennikov, and V. V. Ivanov, "Albian–Cenomanian Orogenic Belt and Igneous

Province of Pacific Asia," Russ. J. Pac. Geol. **13** (3), 187–219 (2019).

29. N. L. Sharpenok, A. E. Kostin, and E. A. Kukharenko, "Total alkali–silica TAS-diagram for chemical classification and identification of plutonic rocks," Reg. Geol. Metallog., No. 56, 40–50 (2013).
30. L. R. Black, S. L. Kamo, C. M. Allen, J. N. Heinikoff, D. W. Dawis, J. Russell, R. J. Korsch, and C. Foudonlis, "TEMORA 1: a new zircon standard for U-Pb geochronology," Chem. Geol. **200**, 155–170 (2003).
31. W. V. Boynton, "Geochemistry of rare earth elements: meteorite studies," Ed. by P. Henderson, *Rare Earth Elements Geochemistry* (Elsevier: Acad. Press, 1984), pp. 63–114.
32. B. W. Chappel and A. J. R. White, "Two contrasting granite types," Pacific Geol., No. 8, 173–174 (1984).
33. B. R. Frost, C. G. Barnes, W. J. Collins, R. J. Arculus, D. J. Ellis, and C. D. Frost, "A geochemical classification for granitic rocks," J. Petrol. **42** (11), 2033–2048 (2001).
34. R. W. Le Maitre, *Classification of Igneous Rocks and Glossary of Terms: Recommendations of the International Union of Geological Sciences, Subcommission on the Systematics of Igneous Rocks* (Blackwell, Oxford, 1989).
35. K. R. Ludwig, "User's manual for Isoplot/Ex, version 2.10. A geochronological toolkit for Microsoft Excel," Berkeley Geochronol. Center Spec. Publ, No. 1, 2455 (1999).
36. K. R. Ludwig, "SOUID 1.00. A users manual," Berkeley Geochronol. Center Spec. Publ, No. 2, 2455 (2000).
37. J. Maeda, "Opening of the Kuril Basin deduced from the magmatic history of Central Hokkaido, North Japan," Tectonophys. **174**, 235–255 (1990).
38. P. D. Maniar and P. M. Piccoli, "Tectonic discrimination of granitoids," Geology **101** (5), 635–643 (1989).
39. J. A. Pearce, N. B. W. Harris, and A. G. Tindle, "Trace element discrimination diagrams for the tectonic interpretation of granitic rock," J. Petrol. **25**, 956–983 (1984).
40. P. C. Rickwood, "Boundary lines within petrologic diagrams which use oxides of major and minor elements," Lithos **22**, 247–263 (1989).
41. H. Rollinson, *Using Geochemical Data: Evaluation, Presentation, Interpretation* (Longman Scientific and Technical, London, 1993).
42. S. Sun and W. F. McDonough, "Chemical and isotopic systematics of oceanic basalt: implication for mantle composition and processes," *Magmatism in the Ocean Basins*, Ed. by A. D. Saunders and M. J. Norry, Geol. Soc. Spec. Publ. No. 42, 313–345 (1989).
43. S. R. Taylor and S. M. McLennan, *The Continental Crust: Its Evolution and Composition* (Blackwell, London, 1985).
44. J. B. Whalen, K. L. Currie, and B. W. Chappell, "A-type granites: geochemical characteristics, discrimination and petrogenesis," Contrib. Mineral. Petrol. **95** (4), 407–419 (1987).
45. I. S. Williams, "U-Th-Pb geochronology by ion microprobe: applications of microanalytical techniques to understanding mineralizing processes," Rev. Econ. Geol. **79**, 169–181 (1998).
46. http://geochron.vsegei.ru/.

Recommended for publishing by A.I. Khanchuk
Translated by M. Bogina